Measurements of H$\rightarrow \tau\tau$ cross-section at FCC-ee

S. Giappichini[1], M. Klute[1], M. Presilla[1], A. Wiedl[1], X. Zuo[1], and M. Cepeda[2]

[1]Institute for Experimental Particle Physics (ETP), Karlsruhe Institute of Technology (KIT), Wolfgang-Gaede-Straße 1, D-76131, Karlsruhe, Germany
[2]CIEMAT, Avenida Complutense 40, 28040, Madrid, Spain

Contents

1 Introduction

The Higgs boson is a central piece of our current understanding of fundamental particle physics and, in turn, of the Standard Model (SM). After its discovery in 2012 [1, 2], the rich experimental program of associated measurements aimed at exploring its properties as well as getting hints of new physics beyond the weak scale (beyond the Standard Model, BSM).

The e^+e^- Future Circular Collider (FCC-ee) [3] is a new Higgs factory proposed to be built at CERN in the coming years. The core of the FCC-ee program is to measure Higgs production inclusively [4]. This setup would result in a clean environment, without pile-up collisions, underlying events, and a much larger signal-to-background ratio than at the Large Hadron Collider (LHC), thus potentially achieving better results in less time.

The goal of this study is to estimate the achievable relative uncertainty on the cross-section of the Higgs decay into a pair of taus in the ZH production channel at FCC-ee at $\sqrt{s} = 240$ GeV, where circa 2×10^6 ZH events are expected in two years of operation. Additional opportunities are present and studied in this work, regarding the operation at $\sqrt{s} = 365$ GeV, where the W vector boson fusion (VBF) process becomes relevant alongside the ZH associated production.

The work is based on a fast simulation of the IDEA detector concept [5], one of the main designs proposed for FCC-ee based on a short-drift wire chamber and a dual-readout calorimeter. We consider three main variables to reconstruct the invariant mass of the $H \to \tau\tau$ system. Firstly, the invariant mass of the tau pair can be calculated using the collinear approximation [6]. Secondly, the recoil mass, M_{recoil}, of the system recoiling against the lepton pair is calculated from the momenta of the decay products of the Z and the total energy-momentum conservation:

$$M^2_{recoil} = s + M^2_Z - 2\sqrt{s}(E_1 + E_2), \tag{1}$$

where $\sqrt{s}$ is the center of mass energy, E_i are the energies of the Z decay products. Finally, the invariant mass of the visible decay products of the taus forms the visible mass of the di-tau system, $M_{visible}$. These variables help differentiate $H \to \tau\tau$ decays from background processes. The first option is the most precise in visible Z decay channels, as it accounts for the missing energy coming from the tau decay. The second is not as accurate if the recoil system is not well determined, while the final option is usually the worst-performing but the only one accessible for invisible Z decay. Both a traditional cut-based event selection and the performance of a boosted decision tree (BDT) have been studied to increase the signal purity, and, in turn, the achievable precision on the measurement.

2 Event simulation and reconstruction

Signal and background processes have been produced by the FCC-ee event generation contact in the "Winter 2023" production campaign [7, 8] in the EDM4hep format [9]. Most samples have been generated with Whizard v. 3.0.3 [10, 11], including a parameterization of initial state radiation. Subsequently, Pythia6 [12] was used to hadronize the initial and final states. In the other cases, Pythia8 took care of both steps. Delphes v. 3.5.1pre05 [13] simulated the response of the IDEA detector [5]. The analysis framework employed is common to all FCC analyses [14].

FastJet [15] is responsible for reconstructing jets. We tested two jet algorithms: the e^+e^- inclusive generalized k_t algorithm with the jet-radius parameter equal to $R = 0.5$ and a cut on the merging scale of $p_{T,j} > 2$ GeV, and the e^+e^- exclusive Durham algorithm with n_{jets} equal to the expected number of jets. Isolated electrons and muons, with $p > 20$ GeV and isolation lower than 0.25, have been removed from the list of possible jet constituents. We noticed that in both cases, the algorithms would cluster single photons as jets in about 1% of the events. These single-photon cases have been removed from the list of jets.

A fundamental step in the analysis is the reconstruction of the Higgs boson via the taus. Leptonic taus decays are identified by looking directly at the isolated leptons in the event. For the hadronic decays, comprising about 65% of the cases, we have compared two reconstruction methods based on the initial reconstruction of jets in the events:

- **Explicit tau reconstruction**

  Jets containing electrons or muons are immediately tagged as quark jets. For the remaining, the four-vector of the taus, along with the charge (± 1) and mass, are based on the constituents spatially close ($\Delta R < 0.2$) to the leading charged pion of the jet. The number of charged pions and photons, in conjunction with a further selection on the total mass being below 3 GeV, is used to infer the tau decay mode, assigning a separate value to the rejected jets.

- **ParticleNet tau reconstruction**

  We have also investigated how a ParticleNet algorithm, trained on di-jet Higgs events for FCC-ee [16], performs in this analysis. In this instance, the tau jets are defined by a tau score above 0.5, while quark jets did not meet this criterion.

We targeted the following combinations of Z and Higgs boson decays in the ZH channel:

- Z$\rightarrow \ell\ell$ with $\ell = e, \mu$,
- Z$\rightarrow qq$ with q=u, d, s, b, c,
- Z$\rightarrow \nu\nu$,
- $H \rightarrow \tau_\ell \tau_\ell$,
- $H \rightarrow \tau_\ell \tau_h$,
- $H \rightarrow \tau_h \tau_h$,

where τ_ℓ denotes leptonic taus decays and τ_h hadronic decays. For the VBF channel, we analyzed all three $H \rightarrow \tau\tau$ decay modes. The decay of $Z \rightarrow \tau\tau$ in ZH processes has been considered as background. In this way, we have nine orthogonal categories based on the final state objects.

If more than two leptons are present in the final state, we considered the pair with opposite charge, same flavor, and invariant mass closest to 91 GeV to reconstruct the Z boson and assigned the others to the tau leptonic decays. For the two categories where we expect no jets, only the inclusive jet reconstruction has been employed. The scaled number of events after the object selection can be found in Appendix F.

3 Cross-section at $\sqrt{s}$ =240 GeV

Tab.1 shows the tau reconstruction efficiency calculated for all combinations of tau reconstruction and jet algorithms by looking for reconstructed taus with $\Delta R < 0.2$ from the true hadronic taus. No other selection criteria were applied for this study. As one could expect, the performance is worse in the $Z \rightarrow qq$ samples since there is more overlap between quark and tau jets. The inclusive jet clustering has higher efficiency than the exclusive clustering in all cases. For non-hadronic Z decays, the best efficiency comes from the ParticleNet tau reconstruction and from the explicit reconstruction in the other cases, although they are comparable.

	Explicit tau reconstruction		ParticleNet tau reconstruction	
	Inclusive jets	Exclusive jets	Inclusive jets	Exclusive jets
$Z \to \nu\nu,\ H \to \tau\tau$	90.34%	87.09%	97.60%	94.20%
$Z \to ee,\ H \to \tau\tau$	84.96%	78.07%	95.15%	83.21%
$Z \to \mu\mu,\ H \to \tau\tau$	84.96%	79.94%	95.15%	87.37%
$Z \to bb,\ H \to \tau\tau$	77.69%	77.31%	76.23%	65.72%
$Z \to cc,\ H \to \tau\tau$	78.45%	78.07%	76.58%	65.72%
$Z \to ss,\ H \to \tau\tau$	78.82%	78.07%	76.15%	65.50%
$Z \to qq,\ H \to \tau\tau$	78.78%	77.95%	76.57%	65.50%

Table 1: Efficiency of hadronic tau decay reconstruction at $\sqrt{s} = 240$ GeV. The values correspond to matching the reconstructed tau to the generated one in a cone of ΔR <0.2 rad. For the exclusive jet algorithm, the efficiency is calculated by considering $n_{jets} = 2$ for the leptonic Z decays and $n_{jets} = 4$ for the hadronic ones.

3.1 Event selection

After the basic event selection to define the categories, we studied the performance of event selection to reduce the signal-to-background ratio. These cuts only differ between the visible and invisible Z decays as we have not optimized them further, finding that this did not have a significant effect on the measurement. Tab. 2, and 3 describe the selection steps in detail. The figures in Appendix A show some of the variables of interest in different categories after applying the corresponding cuts. We have noticed that the reconstructed Z mass, and consequently the recoil mass, in the $Z \to qq$ categories does not peak at the expected values due to suboptimal jet clustering.

Cut description for $Z \to \ell\ell$ and $Z \to qq$	Values
1. Selection for $Z \to \ell\ell$	Two leptons with same flavor and opposite charges, two taus with opposite charges*
1. Selection for $Z \to qq$	Two jets and two taus with opposite charges*
2. Collinear mass	$100 < M_{collinear} < 150$ GeV
3. Recoil mass	$115 < M_{recoil} < 160$ GeV
4. Reconstructed Z mass	$70 < M_Z < 100$ GeV
5. Angular distance between taus	$\Delta R_{\tau\tau} > 2$
6. Cosine of the angle between taus	$\cos\theta_{\tau\tau} < -0.6$
7. Cosine of missing theta	$\lvert\cos \not\theta\rvert < 0.98$

Table 2: Table of subsequent cuts applied on the signal and background events in the $Z \to \ell\ell$ and $Z \to qq$ categories at $\sqrt{s} = 240$ GeV. The requirement on the tau charge is only applied in the case of explicit reconstruction.

Cut description for $Z \to \nu\nu$	Values
1. Selection	Two taus with opposite charges*
2. Missing energy	$\not{E} > 100$ GeV
3. Missing rapidity	$\lvert \not{y} \rvert < 1$
4. Azimuthal angle between taus	$\lvert \Delta\phi_{\tau\tau} \rvert < 3$
5. Angular distance between taus	$\Delta R_{\tau\tau} > 2$
6. Cosine of the angle between taus	$\cos\theta_{\tau\tau} < -0.4$
7. Cosine of missing theta	$\lvert \cos\not{\theta} \rvert < 0.98$

Table 3: Table of subsequent cuts applied on the signal and background events in the $Z \to \nu\nu$ categories at $\sqrt{s} = 240$ GeV. The requirement on the tau charge is only applied in the case of the explicit reconstruction.

3.2 BDT classifier

We trained different BDT classifiers in some categories where the number of events is sufficiently high and the separation between signal and backgrounds from the event selection in Sec. 3.1 is not optimal. In particular, a BDT was trained in each sub-category of $Z \to qq$ and $Z \to \nu\nu$ decays to focus it on the specific kinematics. For $Z \to qq$ the BDT has been trained and then applied on events with $100 < M_{collinear} < 150$ GeV, while for $Z \to \nu\nu$ the events had $\not{E} > 100$ GeV. The full list of variables used for the training can be found in Appendix B.

The number of events for each process used in the training reflects the expected number of events in ZH collisions at FCC-ee. The signal samples limit this value and, from the sets built in this way, 70% of the events are used for training while the remaining are used for testing. We trained BDTs with a size of 200 trees and a depth of two. We have not excluded the training set in the final analysis as we do not observe significant over-training, as shown by the signal and background efficiencies in Appendix C. Fig. 1 shows the receiver operating characteristic (ROC) curves for each of the training that was used in the analysis in two of the tau reconstruction methods.

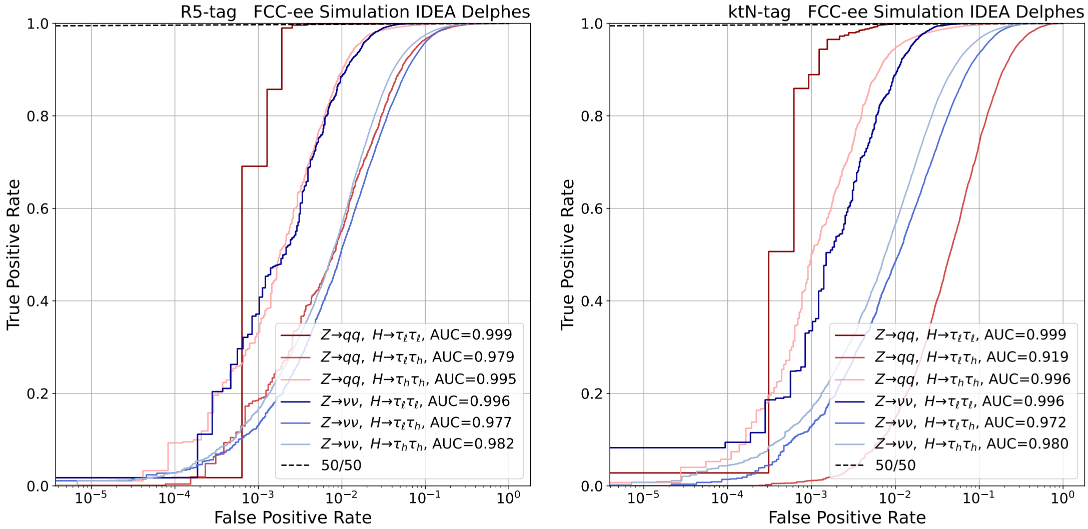

Figure 1: ROC curves for each BDT training and corresponding area under the curve (AUC) value at $\sqrt{s} = 240$ GeV. On the right: ParticleNet tau reconstruction with exclusive jets. On the left: ParticleNet tau reconstruction with inclusive jets.

3.3 Results

We consider two parallel approaches for signal extraction, the "cut-based analysis" and "BDT analysis". The cut-based analysis considers events selected by the criteria described in Sec. 3.1 and evaluates signal strength with fits on kinematic variables: recoil mass for the $Z \to \ell\ell$ and $Z \to qq$ categories, and visible mass for $Z \to \nu\nu$ categories. The BDT analysis takes the BDT outputs derived from Sec. 3.2, where applicable, instead of kinematic variables for signal extraction. In particular, BDTs are not trained in the $Z \to \ell\ell$ categories, for which the fits on recoil mass are included in the so-called BDT analysis.

The relative cross-section uncertainty has been computed by analyzing the discriminating variables in a shape-based analysis with the CMS Combine tool [17]. Statistical uncertainties in the model are handled automatically by the software using the Barlow-Beeston-lite technique [18]. We also consider log-normal uncertainties on the cross-section of the background processes $e^+e^- \to ZZ$, $e^+e^- \to WW$, Drell-Yan, ZH, and photon-induced processes. A comparison between the results from the cut-based analysis and those from BDT anlaysis is detailed in App. E. As the BDT approach presents better precision, it is considered the nominal result.

Table 4 lists the relative precision for the ZH signal under different assumptions for background systematic uncertainties. The leading uncertainty is the signal uncertainty itself. The statistical uncertainty from the finite size of the simulated samples also has a visible impact. Instead, the choice of background normalization uncertainties does not make a visible change in the results.

At FCC-ee, all relevant background processes are expected to be measured with a better than 1% precision. We then chose the nominal scenario for systematic uncertainty for the 240 GeV analysis to be 1% normalization uncertainty for each background process and no statistical uncertainty from the finite number of simulated events. The corresponding relative precision is 0.58% for $\sigma_{ZH} \times \mathcal{B}(H \to \tau\tau)$ at $\sqrt{s} = 240$ GeV with $\mathcal{L}_{int} = 10.8\ \text{ab}^{-1}$.

	Explicit tau reconstruction		ParticleNet tau reconstruction	
	Inclusive jets	Exclusive jets	Inclusive jets	Exclusive jets
WW, ZZ 2%, ZH 20%, others 20%	±0.92%	±0.78%	±0.71%	±0.63%
WW, ZZ 1%, ZH 20%, others 20%	±0.92%	±0.78%	±0.71%	±0.63%
WW, ZZ 1%, ZH 20%, others 1%	±0.91%	±0.77%	±0.71%	±0.63%
WW, ZZ 1%, ZH 5%, others 1%	±0.92%	±0.77%	±0.71%	±0.63%
WW, ZZ 1%, ZH 1%, others 1%	±0.92%	±0.77%	±0.71%	±0.63%
No MC stats, bkg norm unc 1%	±0.87%	±0.71%	±0.66%	±0.58%

Table 4: Relative uncertainty from the BDT-based analysis on $\sigma_{ZH} \times \mathcal{B}(H \to \tau\tau)$ expected from FCC-ee data at $\sqrt{s} = 240$ GeV with $\mathcal{L}_{int} = 10.8$ ab^{-1} form the different selection criteria and tau reconstructions explored. The first column lists the systematic uncertainties set on WW, ZZ, ZH, and other backgrounds. Statistical uncertainty is included in all rows except the last.

4 Cross-section at $\sqrt{s}$ =365 GeV

Tab. 5 shows the tau reconstruction efficiency calculated for all combinations of tau reconstruction and jet algorithm by looking for reconstructed taus within $\Delta R < 0.2$ from the generated hadronic taus. Similar conclusions to the $\sqrt{s} = 240$ GeV case can be made here.

	Explicit tau reconstruction		ParticleNet tau reconstruction	
	Inclusive jets	Exclusive jets	Inclusive jets	Exclusive jets
$Z \to \nu\nu,\ H \to \tau\tau$	90.98%	87.68%	97.97%	92.93%
$Z \to ee,\ H \to \tau\tau$	88.77%	78.90%	96.69%	79.40%
$Z \to \mu\mu,\ H \to \tau\tau$	89.71%	80.73%	97.30%	84.72%
$Z \to bb,\ H \to \tau\tau$	86.31%	80.53%	89.18%	76.60%
$Z \to cc,\ H \to \tau\tau$	86.53%	80.60%	88.93%	76.33%
$Z \to ss,\ H \to \tau\tau$	86.56%	80.63%	88.95%	75.97%
$Z \to qq,\ H \to \tau\tau$	86.56%	80.56%	88.95%	76.28%

Table 5: Efficiency of hadronic tau decay reconstruction at $\sqrt{s} = 365$ GeV. The values correspond to matching the reconstructed tau to the generated one in a cone of ΔR <0.2 rad. For the exclusive jet algorithm, the efficiency is calculated by considering $n_{jets} = 2$ for the leptonic Z decays and $n_{jets} = 4$ for the hadronic ones.

4.1 Event selection

Tab. 6, and 7, describe the cuts applied in detail, which are only marginally different than at $\sqrt{s} = 240$ GeV to account for the different kinematics.

At this energy, we expect a sizable contribution in the $\nu\nu\tau\tau$ final state to come from the vector boson fusion (VBF) channel. The major differences between VBF and ZH kinematics are in the missing transverse momentum and missing mass. We then treat this process separately from ZH events and build the subsequent analysis accounting for the two signal processes.

Cut description for $Z \to \ell\ell$ and $Z \to qq$	Values
1. Selection for $Z \to \ell\ell$	Two leptons with same flavor and opposite charges, two taus with opposite charges*
1. Selection for $Z \to qq$	Two jets and two taus with opposite charges*
2. Collinear mass	$100 < M_{collinear} < 150$ GeV
3. Recoil mass	$115 < M_{recoil} < 160$ GeV
4. Reconstructed Z mass	$70 < M_Z < 100$ GeV
5. Angular distance between taus	$\Delta R_{\tau\tau} > 1$
6. Cosine of the angle between taus	$\cos\theta_{\tau\tau} < 0.25$
7. Cosine of missing theta	$\lvert\cos\not\theta\rvert < 0.98$

Table 6: Table of subsequent cuts applied on the signal and background events in the $Z \to \ell\ell$ and $Z \to qq$ categories at $\sqrt{s} = 365$ GeV. The requirement on the tau charge is only applied in the case of explicit reconstruction.

Cut description for $Z \to \nu\nu$	Values
1. Selection	Two taus with opposite charges*
2. Missing energy	$\not E > 180$ GeV
3. Missing rapidity	$\lvert\not y\rvert < 1$
4. Azimuthal angle between taus	$\lvert\Delta\phi_{\tau\tau}\rvert < 3$
5. Angular distance between taus	$\Delta R_{\tau\tau} > 1$
6. Cosine of the angle between taus	$\cos\theta_{\tau\tau} < 0.25$
7. Cosine of missing theta	$\lvert\cos\not\theta\rvert < 0.98$

Table 7: Table of subsequent cuts applied on the signal and background events in the $Z \to \nu\nu$ categories at $\sqrt{s} = 365$ GeV. The requirement on the tau charge is only applied in the case of the explicit reconstruction.

4.2 BDT classifier

As illustrated in Sec. 3.2, a BDT was trained in each sub-category of $Z \to qq$ decays to focus it on the specific kinematics. In the $\nu\nu$ final states, we have trained a multi-class BDT to also separate the ZH and VBF signatures. For $Z \to qq$ the BDT has been trained and then applied on events with $100 < M_{collinear} < 150$ GeV, while for $\nu\nu$ the events passed the cut $\not E > 180$ GeV. The same variables and strategies as before have been applied here. We have not excluded the training set in the final analysis as we do not observe significant over-training, Appendix D. Fig. 2 shows the ROC curves for the signal-to-background separation for each of the training that was used in the analysis in some of the tau reconstruction methods analyzed. Examples of BDT output distributions are shown in Fig. 3. These distributions are used for the fit described in the next section.

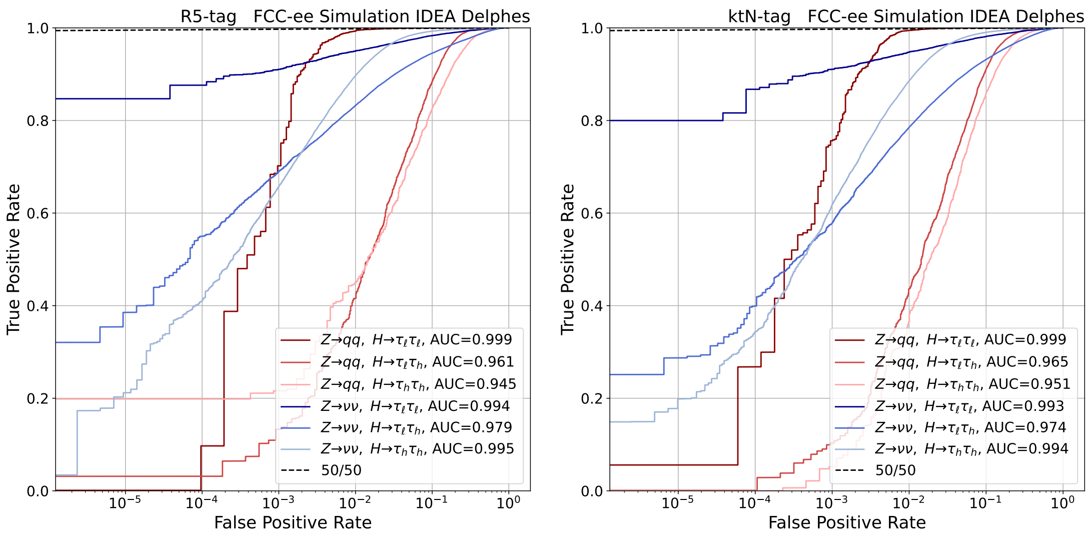

Figure 2: ROC curves for each BDT training, separating the background events from the signal, and corresponding AUC value at $\sqrt{s} = 365$ GeV. On the right: ParticleNet tau reconstruction with exclusive jets. On the left: ParticleNet tau reconstruction with inclusive jets.

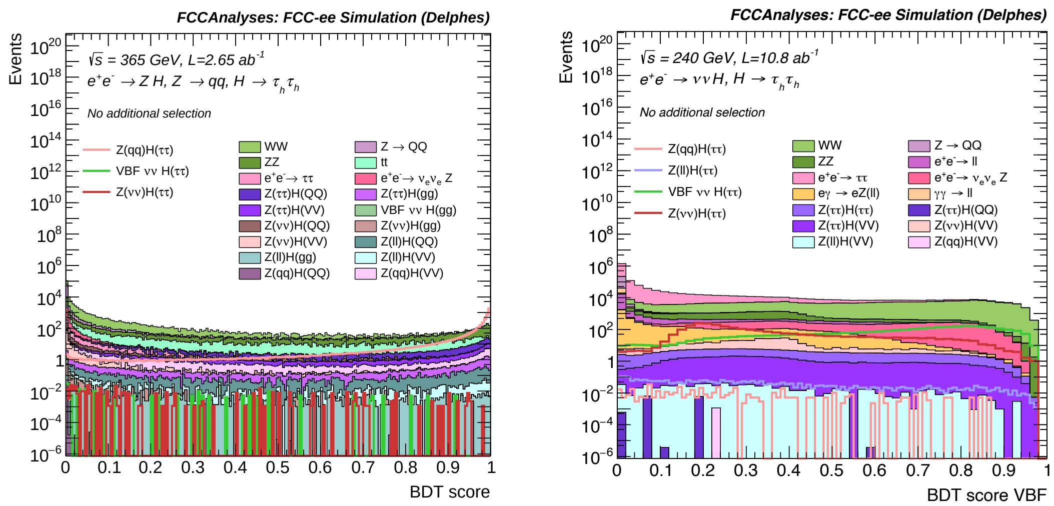

Figure 3: Examples of BDT scores in the $Z \to qq$, $H \to \tau_h\tau_h$ category (left) and in the $Z \to \nu\nu$, $H \to \tau_h\tau_h$ (right) at $\sqrt{s}$ =365 GeV.

4.3 Results

The relative uncertainty for the cross-section measurement at $\sqrt{s} = 365$ GeV has been computed similarly as illustrated in Sec. 3.3. When using BDT classifiers for the event selection, the fit for the trained categories is based on the BDT background score (200 bins) for the $Z \to qq$ categories and on the BDT VBF score (50 bins) for $\nu\nu$ final states to maximize the sensitivity to this signal. A comparison between the results from the cut-based analysis and those from BDT anlaysis is detailed in App. E. As the BDT approach presents better precision, it is considered the nominal result.

Tab. 8 and 9 list the relative precision for ZH and VBF signals, respectively, under different assumptions for background systematic uncertainties. The ZH precision does not depend much on the background uncertainties since the signal is well modeled, as illustrated in the left plot of Fig. 3. The leading uncertainty is, instead, the statistical uncertainty of the signal itself. On the other hand, the VBF precision depends almost solely on the WW uncertainty since the sample used for this analysis contains a limited number of events compared to its cross section, while being the leading background, Fig. 3. This statistical uncertainty from WW simulation makes the precision estimate highly pessimistic (from 13.5% to 25%), while such limitation will not be an issue for actual FCC-ee data. To properly address this systematic uncertainty, more simulation samples will be generated for further evaluation, which is beyond the timescale of this note. For this note, we choose not to consider statistical uncertainty from the current samples as a systematic uncertainty.

The nominal scenario for systematic uncertainty for the $\sqrt{s}$ =365 GeV analysis includes 1% normalization uncertainty for each background process and no statistical uncertainty from the finite size of the simulated events. The corresponding relative precision is ± 1.27% for $\sigma_{ZH} \times \mathcal{B}(H \to \tau\tau)$ and ± 13.54% for $\sigma_{\nu_e\nu_e H} \times \mathcal{B}(H \to \tau\tau)$ expected from FCC-ee at $\sqrt{s} = 365$ GeV with $\mathcal{L}_{int} = 3$ ab^{-1}. Please note that, as discussed above, the treatment of statistical uncertainty from simulation will be revisited in further studies, and the precision for the VBF signal is expected to be re-evaluated.

Including MC stats	Explicit tau reconstruction		ParticleNet tau reconstruction	
	Inclusive jets	Exclusive jets	Inclusive jets	Exclusive jets
WW, ZZ 2%, Higgs 20%, others 20%	±2.11%	±1.57%	±1.69%	±1.32%
WW, ZZ 1%, Higgs 20%, others 20%	±2.11%	±1.57%	±1.69%	±1.32%
WW, ZZ 1%, Higgs 20%, others 1%	±2.11%	±1.57%	±1.68%	±1.32%
WW, ZZ 1%, Higgs 5%, others 1%	±2.11%	±1.57%	±1.68%	±1.31%
WW, ZZ 1%, Higgs 1%, others 1%	±2.09%	±1.57%	±1.69%	±1.33%

No MC stats	Explicit tau reconstruction		ParticleNet tau reconstruction	
	Inclusive jets	Exclusive jets	Inclusive jets	Exclusive jets
WW, ZZ 2%, Higgs 20%, others 20%	±2.02%	±1.45%	±1.62%	±1.27%
WW, ZZ 1%, Higgs 20%, others 20%	±2.01%	±1.45%	±1.62%	±1.28%
WW, ZZ 1%, Higgs 1%, others 1%	±2.02%	±1.44%	±1.62%	±1.27%
No bkg syst (0.01% for all)	±2.02%	±1.45%	±1.62%	±1.26%

Table 8: Relative uncertainty from the BDT-based analysis on $\sigma_{ZH} \times \mathcal{B}(H \to \tau\tau)$ expected from FCC-ee data at $\sqrt{s} = 365$ GeV with $\mathcal{L}_{int} = 3$ ab^{-1} form the different selection criteria and tau reconstructions explored. Different assumptions on background uncertainties are tested. The first table shows results considering statistical uncertainty from finite simulation samples. The second table does not consider simulation statistical uncertainty. The first column lists the systematic uncertainties set on WW, ZZ, ZH, and other backgrounds.

Including MC stats	Explicit tau reconstruction		ParticleNet tau reconstruction	
	Inclusive jets	Exclusive jets	Inclusive jets	Exclusive jets
WW, ZZ 2%, Higgs 20%, others 20%	±25.01%	±28.58%	±20.83%	±25.05%
WW, ZZ 1%, Higgs 20%, others 20%	±25.84%	±28.57%	±22.24%	±24.60%
WW, ZZ 1%, Higgs 20%, others 1%	±25.84%	±28.28%	±22.22%	±25.01%
WW, ZZ 1%, Higgs 5%, others 1%	±25.70%	±28.58%	±22.26%	±25.03%
WW, ZZ 1%, Higgs 1%, others 1%	±25.83%	±28.58%	±22.30%	±25.04%

No MC stats	Explicit tau reconstruction		ParticleNet tau reconstruction	
	Inclusive jets	Exclusive jets	Inclusive jets	Exclusive jets
WW, ZZ 2%, Higgs 20%, others 20%	±14.17%	±15.55%	±12.17%	±13.60%
WW, ZZ 1%, Higgs 20%, others 20%	±14.20%	±15.61%	±12.16%	±13.68%
WW, ZZ 1%, Higgs 1%, others 1%	±14.04%	±15.63%	±12.00%	±13.54%
no bkg syst (0.01% for all)	±13.43%	±15.09%	±12.17%	±13.50%

Table 9: Relative uncertainty from the BDT-based analysis on $\sigma_{\nu_e\nu_e H} \times \mathcal{B}(H \to \tau\tau)$ expected from FCC-ee at $\sqrt{s} = 365$ GeV with $\mathcal{L}_{int} = 3$ ab^{-1} with the different selection criteria and tau reconstructions explored. Different assumptions on background uncertainties are tested. The first table shows results considering statistical uncertainty from finite simulation samples, while the second does not. The first column lists the systematic uncertainties set on WW, ZZ, ZH, and other backgrounds.

5 Conclusions

In this document, we have presented a first analysis of the expected $H \to \tau\tau$ relative cross-section uncertainty in the ZH associated production channel at $\sqrt{s} = 240$ GeV and from ZH and vector boson fusion production modes at $\sqrt{s} = 365$ GeV for the e^+e^- Future Circular Collider (FCC-ee). We achieved this result with a fast simulation of the IDEA detector concept including all relevant background events and decay modes. We have also developed an algorithm to reconstruct hadronic tau decays that we compared to a ParticleNet algorithm trained to distinguish the jet flavor. Finally, we have employed a BDT classifier to get higher discriminating power between signal and background. We have found that the tau reconstruction from the ParticleNet algorithm, combined with the BDT event selection, resulted in a lower uncertainty on the measurement. The following table 10 gives a summary of our results.

$\sqrt{s}$	240 GeV	365 GeV	
$\mathcal{L}$	10.8 ab^{-1}	3 ab^{-1}	
	ZH	ZH	VBF
$H \to \tau\tau$	±0.58%	±1.27%	±13.54%

Table 10: Summary of the results of this paper. In particular, the second and third columns show the relative uncertainty on $\sigma_{ZH} \times \mathcal{B}(H \to \tau\tau)$, while the last column refers to $\sigma_{\nu_e\nu_e H} \times \mathcal{B}(H \to \tau\tau)$. These values are extracted by considering the ParticleNet tau reconstruction with exclusive jet clustering and a BDT event selection. As discussed in Sec. 4.3, the precision on the $\sigma_{\nu_e\nu_e H} \times \mathcal{B}(H \to \tau\tau)$ signal is preliminary and will be updated with further studies.

A Sample of plots at $\sqrt{s} = 240$ GeV

The following plots use the exclusive jet algorithm and ParticleNet tau reconstruction. Similar plots can be drawn for the other combinations of jet algorithms and tau reconstructions, also at $\sqrt{s} = 365$ GeV.

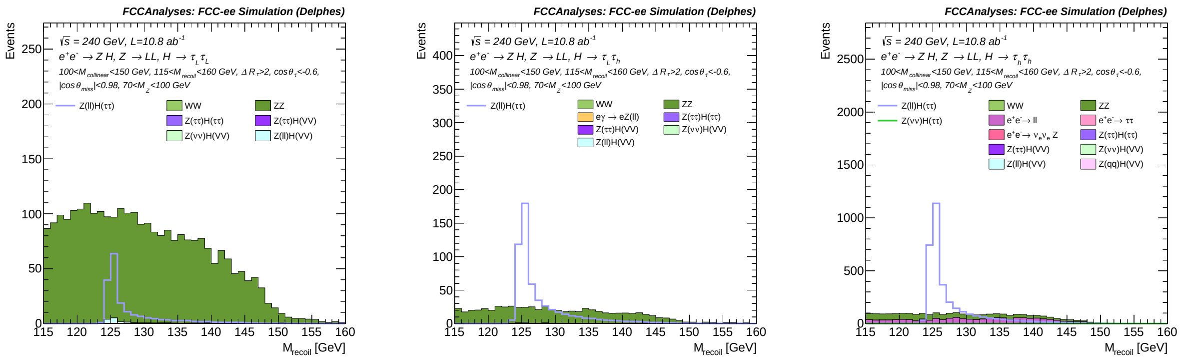

(a) $Z \to \ell\ell$, $H \to \tau_\ell\tau_\ell$. (b) $Z \to \ell\ell$, $H \to \tau_\ell\tau_h$. (c) $Z \to \ell\ell$, $H \to \tau_h\tau_h$.

Figure 4: Reconstructed recoil mass for the decay of $Z \to \ell\ell$ and the combinations of tau decays using an exclusive jet algorithm and ParticleNet tau reconstruction. All signal and background samples are shown, having passed the full set of cuts listed in Tab. 2.

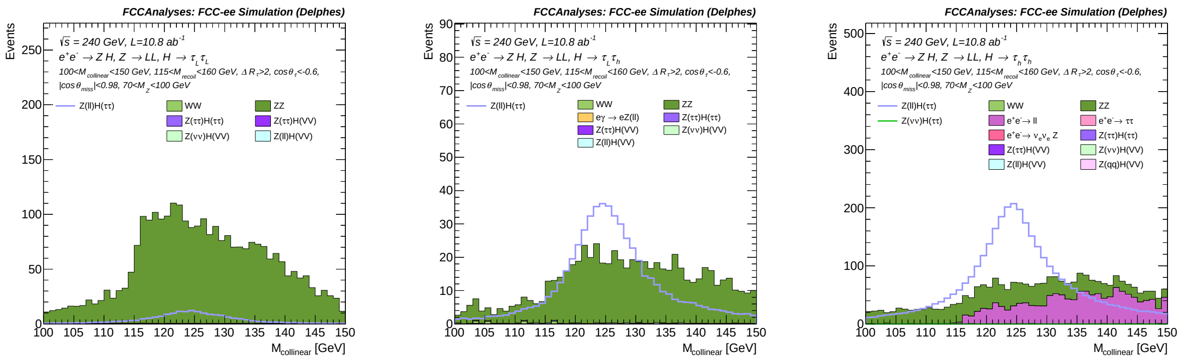

(a) $Z \to \ell\ell$, $H \to \tau_\ell\tau_\ell$. (b) $Z \to \ell\ell$, $H \to \tau_\ell\tau_h$. (c) $Z \to \ell\ell$, $H \to \tau_h\tau_h$.

Figure 5: Reconstructed collinear mass for the decay of $Z \to \ell\ell$ and the combinations of tau decays using an exclusive jet algorithm and ParticleNet tau reconstruction. All signal and background samples are shown, having passed the full set of cuts listed in Tab. 2.

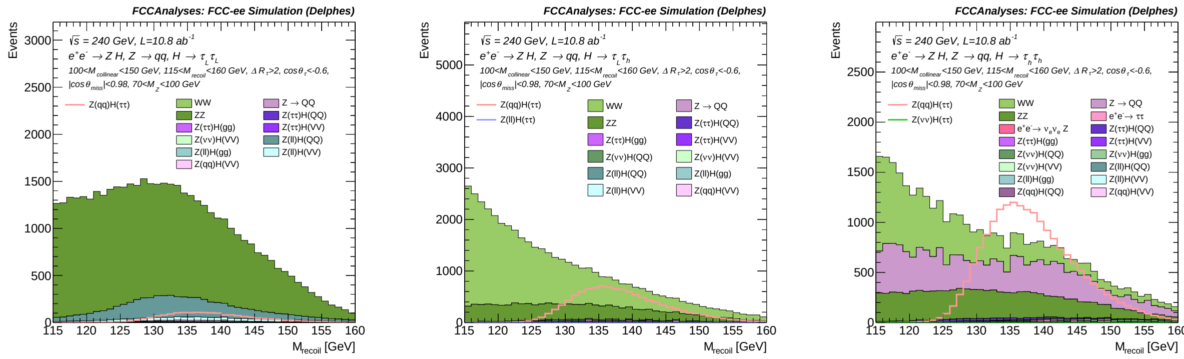

(a) $Z \to qq$, $H \to \tau_\ell\tau_\ell$.

(b) $Z \to qq$, $H \to \tau_\ell\tau_h$.

(c) $Z \to qq$, $H \to \tau_h\tau_h$.

Figure 6: Reconstructed recoil mass for the decay of $Z \to qq$ and the combinations of tau decays using an exclusive jet algorithm and ParticleNet tau reconstruction. All signal and background samples are shown, having passed the full set of cuts listed in Tab. 2.

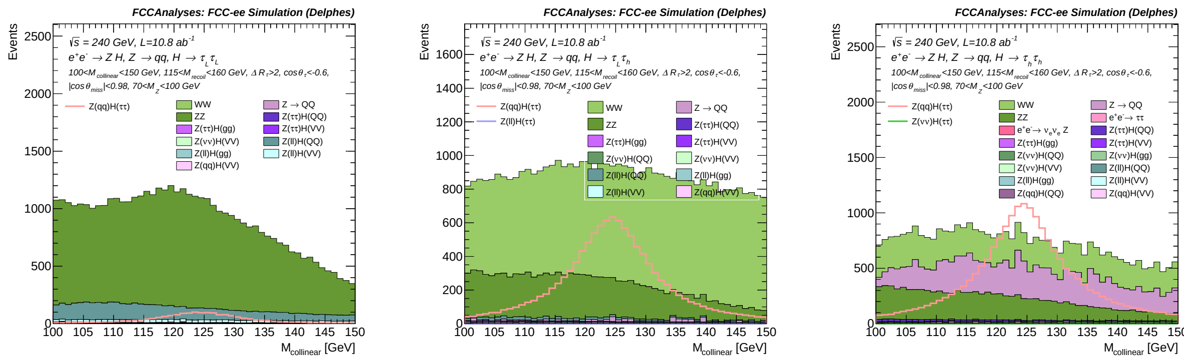

(a) $Z \to qq$, $H \to \tau_\ell\tau_\ell$.

(b) $Z \to qq$, $H \to \tau_\ell\tau_h$.

(c) $Z \to qq$, $H \to \tau_h\tau_h$.

Figure 7: Reconstructed collinear mass for the decay of $Z \to qq$ and the combinations of tau decays using an exclusive jet algorithm and ParticleNet tau reconstruction. All signal and background samples are shown, having passed the full set of cuts listed in Tab. 2.

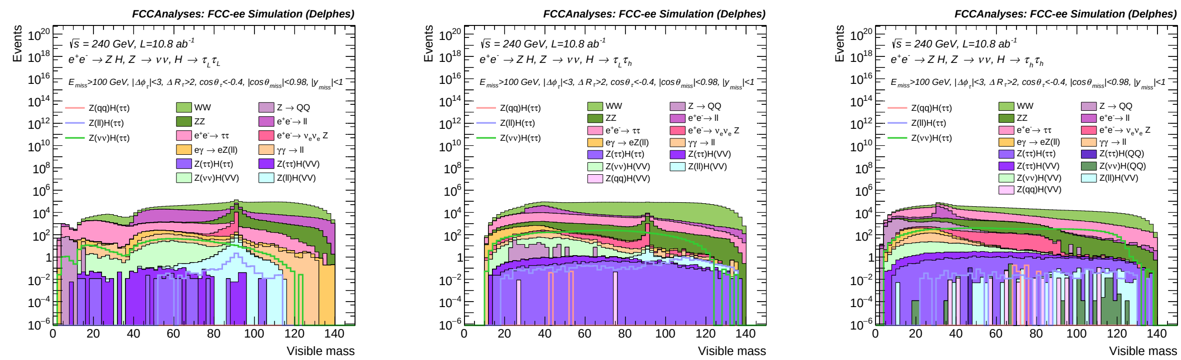

(a) $Z \to \nu\nu$, $H \to \tau_\ell\tau_\ell$.

(b) $Z \to \nu\nu$, $H \to \tau_\ell\tau_h$.

(c) $Z \to \nu\nu$, $H \to \tau_h\tau_h$.

Figure 8: Reconstructed visible mass for the decay of $Z \to \nu\nu$ and the combinations of tau decays using an exclusive jet algorithm and ParticleNet tau reconstruction. All signal and background samples are shown, having passed the full set of cuts listed in Tab. 3.

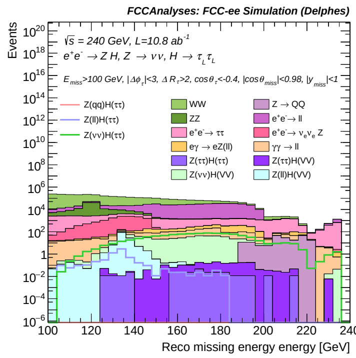

(a) $Z \to \nu\nu$, $H \to \tau_\ell \tau_\ell$.

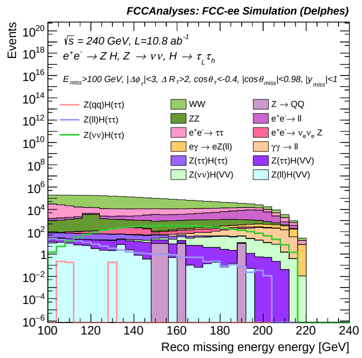

(b) $Z \to \nu\nu$, $H \to \tau_\ell \tau_h$.

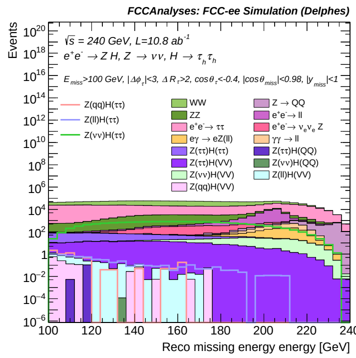

(c) $Z \to \nu\nu$, $H \to \tau_h \tau_h$.

Figure 9: Reconstructed missing energy for the decay of $Z \to \nu\nu$ and the combinations of tau decays using an exclusive jet algorithm and ParticleNet tau reconstruction. All signal and background samples are shown, having passed the full set of cuts listed in Tab. 3.

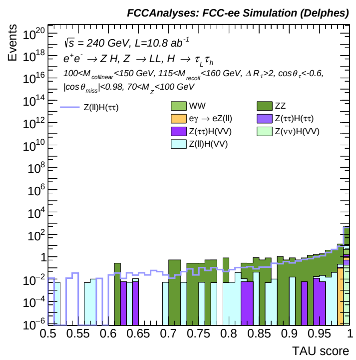

(a) $Z \to \ell\ell$, $H \to \tau_\ell \tau_h$.

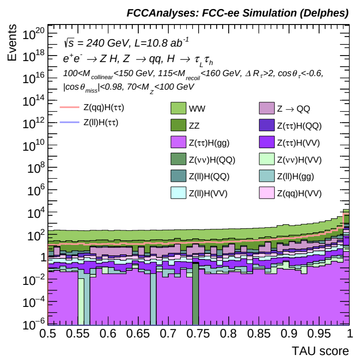

(b) $Z \to qq$, $H \to \tau_\ell \tau_h$.

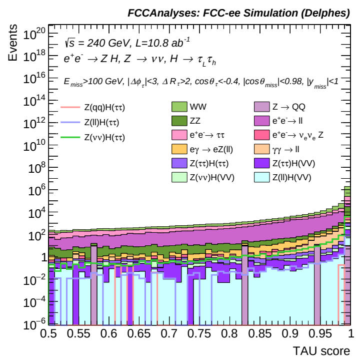

(c) $Z \to \nu\nu$, $H \to \tau_\ell \tau_h$.

Figure 10: Tau score from ParticleNet for the exclusive jets in the events for different Z decays and $H \to \tau_\ell \tau_h$. All signal and background samples are shown, having passed the full set of cuts listed in Tab. 2, 3.

B List of variables for BDT training

The variables used for the BDT training at both energy points are for the $Z \to \nu\nu$ channel:

- RecoEmiss_pz,
- RecoEmiss_pt,
- RecoEmiss_p,
- RecoEmiss_e,
- RecoEmiss_costheta,
- RecoH_pz,
- RecoH_p,
- RecoH_pt,
- RecoH_e,
- RecoH_eta,
- TauLead_pz,
- TauLead_p,
- TauLead_pt,
- TauLead_e,
- TauLead_eta,
- TauLead_mass,
- TauSub_pz,
- TauSub_p,
- TauSub_pt,
- TauSub_e,
- TauSub_eta,

- TauSub_mass,
- Tau_DPhi,
- Tau_DR,
- Tau_cos,
- Tau_DEta,
- Visible_mass.

Similarly, for $Z \to qq$ the list is:

- RecoEmiss_pz,
- RecoEmiss_pt,
- RecoEmiss_p,
- RecoEmiss_e,
- RecoEmiss_costheta,
- RecoZ_pz,
- RecoZ_p,
- RecoZ_pt,
- RecoZ_e,
- RecoZ_eta,
- RecoZ_mass,
- RecoH_pz,
- RecoH_p,
- RecoH_pt,
- RecoH_e,
- RecoH_eta,
- RecoH_mass,
- Tau_DPhi,
- Tau_DR,
- Tau_cos,
- Tau_DEta,
- Recoil,
- Collinear_mass.

To these, TauLead_type (ParticleNet tau score), n_TauLead_charged_constituents, n_TauLead_neutral_constituents, TauSub_type, n_TauSub_charged_constituents, and n_TauSub_neutral_constituents are added when analyzing the ParticleNet reconstruction.

C BDT plots at $\sqrt{s} = 240$ GeV

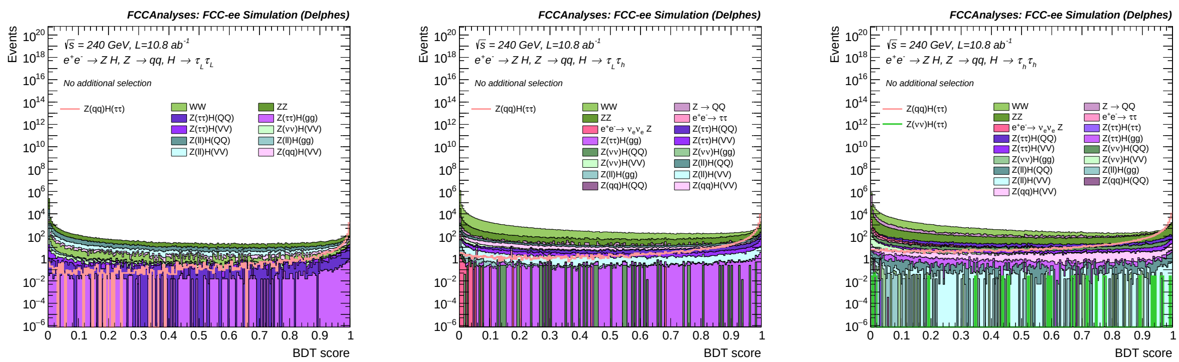

(a) $Z \to qq$, $H \to \tau_\ell \tau_\ell$.
(b) $Z \to qq$, $H \to \tau_\ell \tau_h$.
(c) $Z \to qq$, $H \to \tau_h \tau_h$.

Figure 11: BDT score for the decay of $Z \to qq$ and the combinations of tau decays using an exclusive jet algorithm and ParticleNet tau reconstruction at $\sqrt{s} = 240$ GeV.

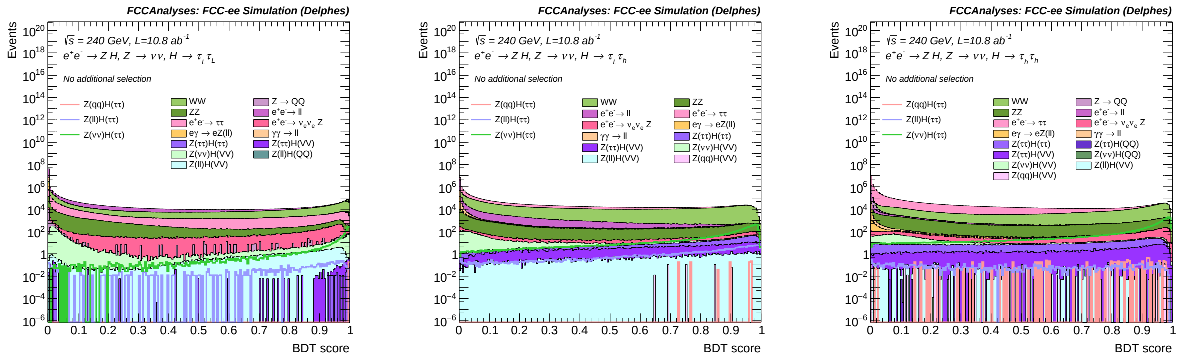

(a) $Z \to \nu\nu$, $H \to \tau_\ell\tau_\ell$. (b) $Z \to \nu\nu$, $H \to \tau_\ell\tau_h$. (c) $Z \to \nu\nu$, $H \to \tau_h\tau_h$.

Figure 12: BDT score for the decay of $Z \to \nu\nu$ and the combinations of tau decays using an exclusive jet algorithm and ParticleNet tau reconstruction at $\sqrt{s} = 240$ GeV.

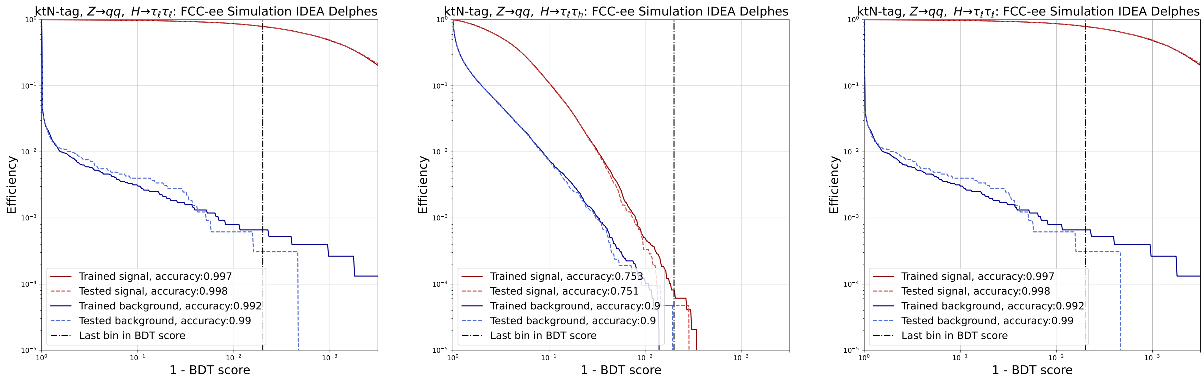

(a) $Z \to qq$, $H \to \tau_\ell\tau_\ell$. (b) $Z \to qq$, $H \to \tau_\ell\tau_h$. (c) $Z \to qq$, $H \to \tau_h\tau_h$.

Figure 13: Overtraining test for the decay of $Z \to qq$ and the combinations of tau decays using an exclusive jet algorithm and ParticleNet tau reconstruction at $\sqrt{s} = 240$ GeV.

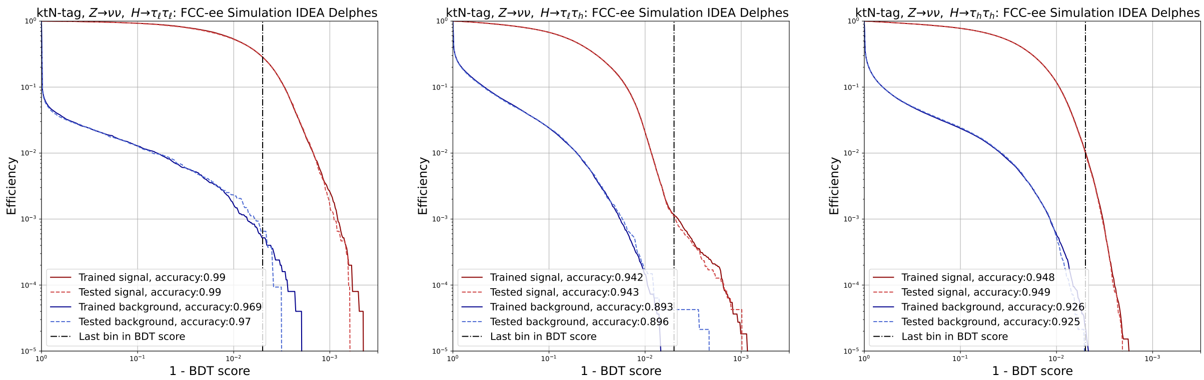

(a) $Z \to \nu\nu$, $H \to \tau_\ell\tau_\ell$. (b) $Z \to \nu\nu$, $H \to \tau_\ell\tau_h$. (c) $Z \to \nu\nu$, $H \to \tau_h\tau_h$.

Figure 14: Overtraining test for the decay of $Z \to \nu\nu$ and the combinations of tau decays using an exclusive jet algorithm and ParticleNet tau reconstruction at $\sqrt{s} = 240$ GeV.

D BDT plots at $\sqrt{s} = 365$ GeV

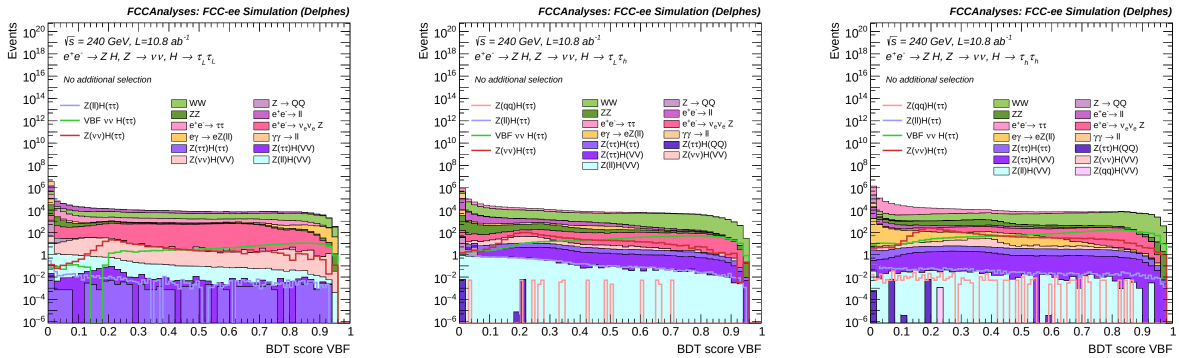

(a) $\nu\nu H$, $H \to \tau_\ell\tau_\ell$.

(b) $\nu\nu H$, $H \to \tau_\ell\tau_h$.

(c) $\nu\nu H$, $H \to \tau_h\tau_h$.

Figure 15: BDT VBF score for the $\nu\nu$ final state and the combinations of tau decays using an exclusive jet algorithm and ParticleNet tau reconstruction at $\sqrt{s} = 365$ GeV.

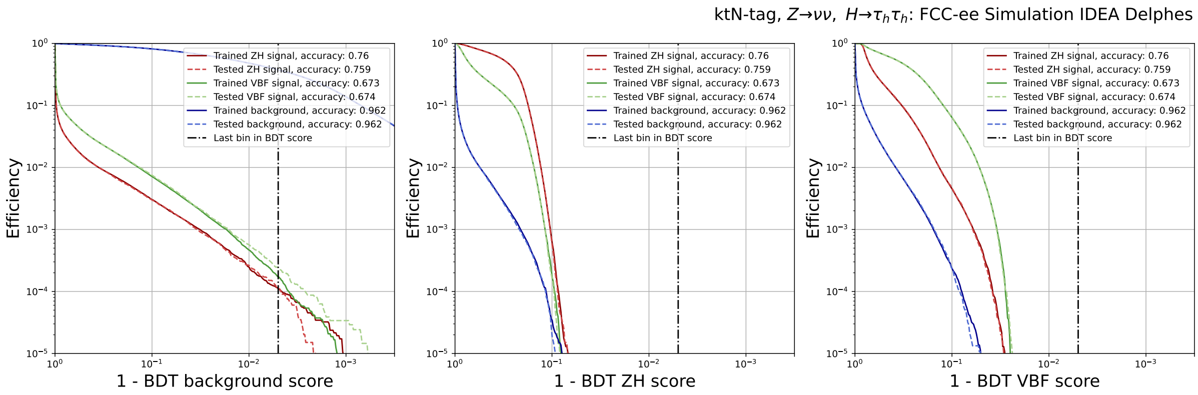

Figure 16: Overtraining tests for $\nu\nu H$, $H \to \tau_h\tau_h$ at $\sqrt{s} = 365$ GeV, using an exclusive jet algorithm and ParticleNet tau reconstruction.

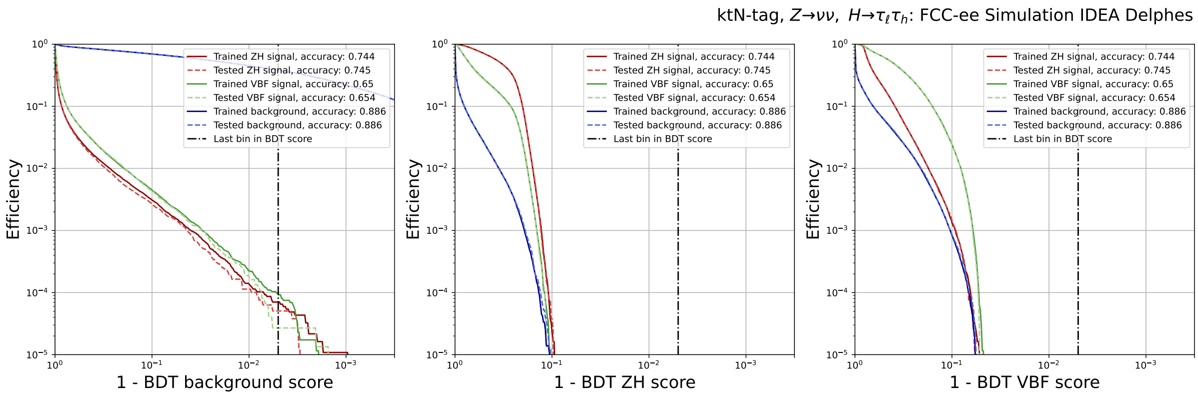

Figure 17: Overtraining tests for $\nu\nu H$, $H \to \tau_\ell\tau_h$ at $\sqrt{s} = 365$ GeV, using an exclusive jet algorithm and ParticleNet tau reconstruction.

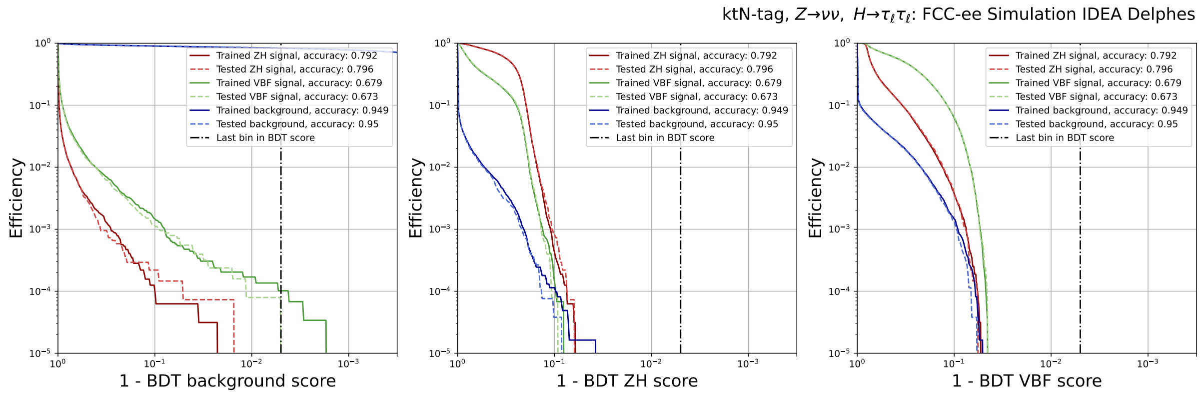

Figure 18: Overtraining tests for $\nu\nu H$, $H \rightarrow \tau_\ell\tau_\ell$ at $\sqrt{s} = 365$ GeV, using an exclusive jet algorithm and ParticleNet tau reconstruction.

E Detailed results for the cross-section uncertainty

Tables 11 to 13 shows the combined fit results for ZH signal at 240 GeV, ZH signal at 365 GeV, and VBF signal at 365 GeV, respectively.

	Explicit tau reconstruction		ParticleNet tau reconstruction	
	Inclusive jets	Exclusive jets	Inclusive jets	Exclusive jets
Cut-based analysis	-1.24 %, +1.25%	±1.49%	-0.90%, +0.91%	±1.01%
BDT analysis	±0.92%	±0.78	±0.71%	±0.63%

Table 11: Relative uncertainty on $\sigma_{ZH} \times \mathcal{B}(H \rightarrow \tau\tau)$ expected from FCC-ee data at $\sqrt{s} = 240$ GeV with $\mathcal{L}_{int} = 10.8$ ab^{-1} form the different selection criteria and tau reconstructions explored. Systematic uncertainties considered are 2% normalization uncertainty on WW and ZZ backgrounds, 20% normalization uncertainty on ZH and other backgrounds, and statistical uncertainty.

	Explicit tau reconstruction		ParticleNet tau reconstruction	
	Inclusive jets	Exclusive jets	Inclusive jets	Exclusive jets
Cut-based analysis	±4.28%	±4.10%	±3.63%	±3.19%
BDT analysis	±2.11%	±1.57%	±1.69%	±1.32%

Table 12: Relative uncertainty on $\sigma_{ZH} \times \mathcal{B}(H \rightarrow \tau\tau)$ expected from FCC-ee data at $\sqrt{s} = 365$ GeV with $\mathcal{L}_{int} = 3$ ab^{-1} form the different selection criteria and tau reconstructions explored. The table shows the sensitivity to ZH events. Systematic uncertainties considered are 2% normalization uncertainty on WW and ZZ backgrounds, 20% normalization uncertainty on ZH and other backgrounds, and statistical uncertainty.

	Explicit tau reconstruction		ParticleNet tau reconstruction	
	Inclusive jets	Exclusive jets	Inclusive jets	Exclusive jets
Cut-based analysis	±25.85%	±25.50%	±23.41%	±24.02%
BDT analysis	±25.01%	±28.58%	±20.83%	±25.05%

Table 13: Relative uncertainty on $\sigma_{\nu_e\nu_e H} \times \mathcal{B}(H \to \tau\tau)$ expected from FCC-ee data at $\sqrt{s} = 365$ GeV with $\mathcal{L}_{int} = 3$ ab^{-1} form the different selection criteria and tau reconstructions explored. Systematic uncertainties considered are 2% normalization uncertainty on WW and ZZ backgrounds, 20% normalization uncertainty on ZH and other backgrounds, and statistical uncertainty.

Tables 14, 15, 16, 17, 18, and 19 consider the following systematic uncertainties: 2% normalization uncertainty on WW and ZZ backgrounds, 20% normalization uncertainty on ZH and other backgrounds, and statistical uncertainty.

	Explicit tau reconstruction			
	Cut-based analysis		BDT analysis	
	Inclusive jets	Exclusive jets	Inclusive jets	Exclusive jets
$Z \to qq,\ H \to \tau_\ell\tau_\ell$	-30.29% , +30.08%	-29.96% , +29.49%	-4.66% , +4.75%	-3.36% , +3.47%
$Z \to qq,\ H \to \tau_\ell\tau_h$	-2.63% , +2.64%	-2.97% , +2.93%	-1.87% , +1.94%	-1.47% , +1.48%
$Z \to qq,\ H \to \tau_h\tau_h$	-2.55% , +2.54%	-7.26% , +7.21%	-1.44% , +1.41%	±1.22%
$Z \to qq$	-1.78% , +1.80%	-2.49% , +2.50%	-1.05% , +1.06%	±0.84%
$Z \to \ell\ell,\ H \to \tau_\ell\tau_\ell$	-16.95% , +17.41%		-	
$Z \to \ell\ell,\ H \to \tau_\ell\tau_h$	-4.42% , +4.54%	-4.10% , +4.18%	-	
$Z \to \ell\ell,\ H \to \tau_h\tau_h$	-2.34% , +2.36%	-1.81% , +1.83%	-	
$Z \to \ell\ell$	-2.02% , +2.08%	-1.66% , +1.67%	-	
$Z \to \nu\nu,\ H \to \tau_\ell\tau_\ell$	-420.15% , +418.79%		-104.80%, +105.46%	
$Z \to \nu\nu,\ H \to \tau_\ell\tau_h$	-54.81% , +54.76%	-59.65% , +59.60%	-12.61% , +12.58%	-13.63% , +13.61%
$Z \to \nu\nu,\ H \to \tau_h\tau_h$	-27.90% , +27.81%	-27.75% , +27.67%	-6.19% , +6.23%	-6.33% , +6.37%
$Z \to \nu\nu$	-10.18% , +10.20%	±10.35%	-4.72% , +4.74%	-4.86% , +4.92%
Combined	-1.24% , +1.25%	±1.49%	±1.03%	±0.82%

Table 14: Relative uncertainty on $\sigma_{ZH} \times \mathcal{B}(H \to \tau\tau)$ expected from FCC-ee at $\sqrt{s} = 240$ GeV with $\mathcal{L}_{int} = 10.8$ ab^{-1} for each of the categories defined in Sec. 2. The ”-” in the table means BDT training are not available for $Z \to \ell\ell$ categories, for which the cut-based results are included in the BDT analysis.

	ParticleNet tau reconstruction			
	Cut-based analysis		BDT analysis	
	Inclusive jets	Exclusive jets	Inclusive jets	Exclusive jets
$Z \to qq,\ H \to \tau_\ell\tau_\ell$	-26.36% , +26.12%	-23.40% , +23.09%	-4.18% , +4.31%	-2.86% , +2.91%
$Z \to qq,\ H \to \tau_\ell\tau_h$	-2.52% , +2.50%	-2.47% , +2.42%	-1.51% , +1.50%	-1.22% , +1.23%
$Z \to qq,\ H \to \tau_h\tau_h$	-1.44% , +1.43%	-2.22% , +2.18%	-1.51% , +1.50%	±0.97%
$Z \to qq$	±1.17%	-1.42% , +1.46%	±0.79%	±0.67
$Z \to \ell\ell,\ H \to \tau_\ell\tau_\ell$	-16.95% , +17.41%		-	
$Z \to \ell\ell,\ H \to \tau_\ell\tau_h$	-4.10% , +4.18%	-5.22% , +5.39%	-	
$Z \to \ell\ell,\ H \to \tau_h\tau_h$	-1.81% , +1.83%	-2.24% , +2.26%	-	
$Z \to \ell\ell$	-1.66% , +1.67%	-2.03% , +2.08%	-	
$Z \to \nu\nu,\ H \to \tau_\ell\tau_\ell$	-420.15%, +418.79%		-104.80%, +105.46%	
$Z \to \nu\nu,\ H \to \tau_\ell\tau_h$	-64.14% , +64.10%	-53.90% , +53.87%	-13.67% , +13.72%	-16.64% , +16.67%
$Z \to \nu\nu,\ H \to \tau_h\tau_h$	-30.33% , +30.19%	-39.76% , +39.59%	-6.15% , +6.13%	-6.27% , +6.31%
$Z \to \nu\nu$	-10.06% , +10.10%	-13.19% , +13.22%	-4.39% , +4.45%	-4.73% , +4.71%
Combined	-0.90%, +0.91%	±1.01%	-0.77%, +0.78%	±0.66%

Table 15: Relative uncertainty on $\sigma_{ZH} \times \mathcal{B}(H \to \tau\tau)$ expected from FCC-ee at $\sqrt{s} = 240$ GeV with $\mathcal{L}_{int} = 10.8$ ab^{-1} for each of the categories defined in Sec. 2. The "-" in the table means BDT training are not available for $Z \to \ell\ell$ categories, for which the cut-based results are included in the BDT analysis.

	Explicit tau reconstruction			
	Cut-based analysis		BDT analysis	
	Inclusive jets	Exclusive jets	Inclusive jets	Exclusive jets
$Z \to qq,\ H \to \tau_\ell\tau_\ell$	-66.03%, +66.19%	-47.14%, +47.05%	-22.80%, +23.05%	-11.98%, +12.11%
$Z \to qq,\ H \to \tau_\ell\tau_h$	-20.69%, +20.56%	-18.14%, +17.93%	-3.86%, +3.94%	-2.71%, +2.73%
$Z \to qq,\ H \to \tau_h\tau_h$	-8.76%, +8.75%	-7.74%, +7.68%	-2.96%, +3.00%	-2.18%, +2.20%
$Z \to qq$	-8.18%, +8.17%	-7.34%, +7.28%	-2.31%, +2.33%	±1.66%
$Z \to \ell\ell,\ H \to \tau_\ell\tau_\ell$	-43.18%, +45.44%		-	
$Z \to \ell\ell,\ H \to \tau_\ell\tau_h$	-10.68%, +11.32%	-12.11%, +12.92%	-	
$Z \to \ell\ell,\ H \to \tau_h\tau_h$	-5.97%, +6.18%	-6.19%, +6.41%	-	
$Z \to \ell\ell$	-5.21%, +5.37%	-5.52%, +5.69%	-	
$Z \to \nu\nu,\ H \to \tau_\ell\tau_\ell$	±235.98%		±212.36%	
$Z \to \nu\nu,\ H \to \tau_\ell\tau_h$	±63.73%	±75.79%	±71.75%	±75.27%
$Z \to \nu\nu,\ H \to \tau_h\tau_h$	±26.11%	±27.25%	±31.15%	±31.68%
$Z \to \nu\nu$	±27.33%	±26.62%	±28.01%	±29.02%
Combined	±4.28%	±4.10%	±2.11%	±1.57%

Table 16: Relative uncertainty on $\sigma_{ZH} \times \mathcal{B}(H \to \tau\tau)$ expected from FCC-ee at $\sqrt{s} = 365$ GeV with $\mathcal{L}_{int} = 3$ ab^{-1} for each of the categories defined in Sec. 2 with explicit tau reconstruction. The "-" in the table means BDT training are not available for $Z \to \ell\ell$ categories, for which the cut-based results are included in the BDT analysis.

	ParticleNet tau reconstruction			
	Cut-based analysis		BDT analysis	
	Inclusive jets	Exclusive jets	Inclusive jets	Exclusive jets
$Z \to qq,\ H \to \tau_\ell \tau_\ell$	-63.23%, +63.32%	-45.10%, +44.97%	-18.75%, +18.93%	-10.96%, +11.08%
$Z \to qq,\ H \to \tau_\ell \tau_h$	-22.63%, +22.48%	-16.82%, +16.64%	-3.24%, +3.29%	-2.36%, +2.38%
$Z \to qq,\ H \to \tau_h \tau_h$	-8.58%, +8.54%	-8.61%, +8.42%	-2.31%, +2.36%	-1.86%, +1.87%
$Z \to qq$	-8.04%, +8.01%	-7.77%, +7.64%	-1.79%, +1.85%	-1.38%, +1.39%
$Z \to \ell\ell,\ H \to \tau_\ell \tau_\ell$	-43.18%, +45.44%		-	
$Z \to \ell\ell,\ H \to \tau_\ell \tau_h$	-9.97%, +10.47%	-13.75%, +14.56%	-	
$Z \to \ell\ell,\ H \to \tau_h \tau_h$	-4.77%, +4.89%	-5.41%, +5.56%	-	
$Z \to \ell\ell$	-4.32%, +4.41%	-5.04%, +5.16%	-	
$Z \to \nu\nu,\ H \to \tau_\ell \tau_\ell$	±235.98%		±208.72%	
$Z \to \nu\nu,\ H \to \tau_\ell \tau_h$	±71.81%	±69.37%	±65.43%	±79.14%
$Z \to \nu\nu,\ H \to \tau_h \tau_h$	±26.42%	±26.55%	±25.71%	±30.04%
$Z \to \nu\nu$	±25.78%	±26.60%	±23.98%	±27.90%
Combined	±3.63%	±3.19%	±1.69%	±1.32%

Table 17: Relative uncertainty on $\sigma_{ZH} \times \mathcal{B}(H \to \tau\tau)$ expected from FCC-ee at $\sqrt{s} = 365$ GeV with $\mathcal{L}_{int} = 3$ ab^{-1} for each of the categories defined in Sec. 2 with ParticleNet tau reconstruction. The "-" in the table means BDT training are not available for $Z \to \ell\ell$ categories, for which the cut-based results are included in the BDT analysis.

	Explicit tau reconstruction			
	Cut-based analysis		BDT analysis	
	Inclusive jets	Exclusive jets	Inclusive jets	Exclusive jets
$\nu_e\nu_e\ H(\to \tau_\ell\tau_\ell)$	±336.67%		±346.25%	
$\nu_e\nu_e\ H(\to \tau_\ell\tau_h)$	±65.40%	±79.74%	±75.64%	±84.15%
$\nu_e\nu_e\ H(\to \tau_h\tau_h)$	±24.84%	±25.29%	±27.94%	±30.38%
$\nu_e\nu_e H$	±25.85%	±25.50%	±25.80%	±28.63%

Table 18: Relative uncertainty on $\sigma_{\nu_e\nu_e H} \times \mathcal{B}(H \to \tau\tau)$ expected from FCC-ee at $\sqrt{s} = 365$ GeV with $\mathcal{L}_{int} = 3$ ab^{-1} for each of the categories defined in Sec. 2 with explicit tau reconstruction.

	ParticleNet tau reconstruction			
	Cut-based analysis		BDT analysis	
	Inclusive jets	Exclusive jets	Inclusive jets	Exclusive jets
$\nu_e\nu_e\ H(\to \tau_\ell\tau_\ell)$	±336.67%		±215.14%	
$\nu_e\nu_e\ H(\to \tau_\ell\tau_h)$	±81.15%	±77.27%	±55.37%	±64.16%
$\nu_e\nu_e\ H(\to \tau_h\tau_h)$	±24.00%	±23.18%	±24.88%	±26.89%
$\nu_e\nu_e H$	±23.41%	±24.02%	±22.07%	±25.06%

Table 19: Relative uncertainty on $\sigma_{\nu_e\nu_e H} \times \mathcal{B}(H \to \tau\tau)$ expected from FCC-ee at $\sqrt{s} = 365$ GeV with $\mathcal{L}_{int} = 3$ ab^{-1} for each of the categories defined in Sec. 3.1 with ParticleNet tau reconstruction.

F Process yields

	$\ell\ell\tau_h\tau_h$	$\ell\ell\tau_\ell\tau_h$	$\ell\ell\tau_\ell\tau_\ell$	$\nu\nu\tau_h\tau_h$	$\nu\nu\tau_\ell\tau_h$	$\nu\nu\tau_\ell\tau_\ell$	$qq\tau_h\tau_h$	$qq\tau_\ell\tau_h$	$qq\tau_\ell\tau_\ell$
ZH ($H\tau\tau$)	2.60e+03	7.84e+02	2.38e+02	1.10e+04	6.69e+03	1.01e+03	1.19e+04	6.63e+03	1.21e+03
ZH ($H \to$ non-$\tau\tau$)	3.00e+02	2.77e+02	6.77e+02	5.64e+02	2.07e+03	2.93e+03	1.64e+04	9.48e+03	3.38e+04
DY	1.98e+03	1.27e+03	1.15e+03	3.31e+07	2.65e+07	2.35e+08	9.02e+06	8.17e+04	1.40e+05
WW	1.83e+02	1.99e+02	4.55e+02	7.41e+05	5.05e+06	8.67e+06	2.17e+06	4.08e+06	2.19e+03
ZZ	2.66e+04	7.90e+03	6.38e+04	7.34e+04	4.39e+04	3.60e+05	1.93e+05	8.85e+04	4.96e+05
$ee \to \nu\nu Z$	0	0	0	4.75e+03	2.37e+03	2.15e+04	2.63e+03	6.65e+00	0
$e\gamma \to eZ$	0	0	1.12e+00	2.05e+02	4.18e+04	2.00e+06	0	1.14e+01	1.04e+03
$\gamma\gamma \to \ell\ell$	0	0	0	5.11e+02	1.03e+05	4.83e+06	0	0	2.22e+01
$\gamma\gamma \to \tau\tau$	0	0	0	0	0	0	0	0	0

Table 20: Table of expected yields of signal and background processes after category selection at $\sqrt{s} = 240$ GeV with $\mathcal{L} = 10.8$ ab^{-1} for explicit tau reconstruction using inclusive jets.

	$\ell\ell\tau_h\tau_h$	$\ell\ell\tau_\ell\tau_h$	$\ell\ell\tau_\ell\tau_\ell$	$\nu\nu\tau_h\tau_h$	$\nu\nu\tau_\ell\tau_h$	$\nu\nu\tau_\ell\tau_\ell$	$qq\tau_h\tau_h$	$qq\tau_\ell\tau_h$	$qq\tau_\ell\tau_\ell$
ZH ($H\tau\tau$)	2.42e+03	6.03e+02	2.38e+02	1.18e+04	7.65e+03	1.01e+03	2.51e+04	1.31e+04	2.09e+03
ZH ($H \to$ non-$\tau\tau$)	5.55e+02	5.04e+02	6.77e+02	3.11e+03	7.99e+03	2.93e+03	7.05e+04	3.36e+04	9.43e+04
DY	2.74e+03	1.19e+02	1.15e+03	3.17e+07	1.88e+07	2.35e+08	8.45e+07	7.16e+05	3.11e+05
WW	2.16e+02	1.60e+02	4.55e+02	1.13e+06	6.39e+06	8.67e+06	7.00e+06	1.19e+07	7.61e+03
ZZ	2.90e+04	5.00e+03	6.38e+04	1.01e+05	5.23e+04	3.60e+05	7.84e+05	1.76e+05	1.00e+06
$ee \to \nu\nu Z$	0	0	0	5.38e+03	1.46e+03	2.15e+04	2.89e+04	6.63e+01	1.26e+00
$e\gamma \to eZ$	0	0	1.12e+00	5.28e+01	1.03e+04	2.00e+06	5.61e-01	3.70e+01	4.41e+03
$\gamma\gamma \to \ell\ell$	0	0	0	8.30e+01	1.29e+04	4.83e+06	0	0	2.98e+01
$\gamma\gamma \to \tau\tau$	0	0	0	0	0	0	0	0	0

Table 21: Table of expected yields of signal and background processes after category selection at $\sqrt{s} = 240$ GeV with $\mathcal{L} = 10.8$ ab^{-1} for explicit tau reconstruction using exclusive jets.

	$\ell\ell\tau_h\tau_h$	$\ell\ell\tau_\ell\tau_h$	$\ell\ell\tau_\ell\tau_\ell$	$\nu\nu\tau_h\tau_h$	$\nu\nu\tau_\ell\tau_h$	$\nu\nu\tau_\ell\tau_\ell$	$qq\tau_h\tau_h$	$qq\tau_\ell\tau_h$	$qq\tau_\ell\tau_\ell$
ZH ($H\tau\tau$)	4.72e+03	1.02e+03	2.38e+02	1.96e+04	8.69e+03	1.01e+03	2.05e+04	9.67e+03	1.11e+03
ZH ($H \to$ non-$\tau\tau$)	8.49e+02	7.19e+02	6.77e+02	2.19e+03	5.51e+03	2.93e+03	1.75e+04	1.69e+04	3.57e+04
DY	4.83e+03	3.17e+02	1.15e+03	5.43e+07	5.79e+07	2.35e+08	6.91e+06	2.72e+05	1.61e+05
WW	4.66e+02	3.93e+02	4.55e+02	1.55e+06	7.25e+06	8.67e+06	1.58e+06	3.98e+06	1.97e+03
ZZ	5.36e+04	2.48e+04	6.38e+04	1.44e+05	1.39e+05	3.60e+05	2.57e+05	2.36e+05	5.86e+05
$ee \to \nu\nu Z$	0	0	0	8.09e+03	4.72e+03	2.15e+04	1.42e+03	1.10e+01	0
$e\gamma \to eZ$	1.03e+03	6.62e+02	1.12e+00	2.54e+04	2.15e+05	2.00e+06	0	0	0
$\gamma\gamma \to \ell\ell$	2.22e+01	0	0	3.08e+04	8.16e+05	4.83e+06	0	0	0
$\gamma\gamma \to \tau\tau$	0	0	0	0	0	0	0	0	0

Table 22: Table of expected yields of signal and background processes after category selection at $\sqrt{s} = 240$ GeV with $\mathcal{L} = 10.8$ ab^{-1} for ParticleNet tau reconstruction using inclusive jets.

	$\ell\ell\tau_h\tau_h$	$\ell\ell\tau_\ell\tau_h$	$\ell\ell\tau_\ell\tau_\ell$	$\nu\nu\tau_h\tau_h$	$\nu\nu\tau_\ell\tau_h$	$\nu\nu\tau_\ell\tau_\ell$	$qq\tau_h\tau_h$	$qq\tau_\ell\tau_h$	$qq\tau_\ell\tau_\ell$
ZH ($H\tau\tau$)	4.60e+03	7.63e+02	2.38e+02	1.89e+04	7.32e+03	1.01e+03	2.79e+04	1.55e+04	2.29e+03
ZH ($H \to$ non-$\tau\tau$)	8.24e+02	4.06e+02	6.77e+02	4.80e+03	5.16e+03	2.93e+03	3.40e+04	3.26e+04	1.05e+05
DY	4.41e+04	3.01e+02	1.15e+03	5.17e+07	4.69e+07	2.35e+08	3.76e+07	4.58e+05	3.26e+05
WW	1.03e+03	2.09e+02	4.55e+02	1.55e+06	5.48e+06	8.67e+06	2.60e+06	6.23e+06	7.31e+03
ZZ	5.85e+04	1.53e+04	6.38e+04	1.81e+05	1.15e+05	3.60e+05	5.90e+05	3.92e+05	1.22e+06
$ee \to \nu\nu Z$	1.26e+00	0	0	7.63e+03	3.40e+03	2.15e+04	1.19e+04	2.43e+01	0
$e\gamma \to eZ$	4.34e+03	3.66e+03	1.12e+00	1.35e+04	1.94e+05	2.00e+06	0	0	0
$\gamma\gamma \to \ell\ell$	2.98e+01	0	0	2.98e+04	4.10e+05	4.83e+06	0	0	0
$\gamma\gamma \to \tau\tau$	0	0	0	0	0	0	0	0	0

Table 23: Table of expected yields of signal and background processes after category selection at $\sqrt{s} = 240$ GeV with $\mathcal{L} = 10.8$ ab^{-1} for ParticleNet tau reconstruction using exclusive jets.

	$\ell\ell\tau_h\tau_h$	$\ell\ell\tau_\ell\tau_h$	$\ell\ell\tau_\ell\tau_\ell$	$\nu\nu\tau_h\tau_h$	$\nu\nu\tau_\ell\tau_h$	$\nu\nu\tau_\ell\tau_\ell$	$qq\tau_h\tau_h$	$qq\tau_\ell\tau_h$	$qq\tau_\ell\tau_\ell$
VBF $H \to \tau\tau$	1.50e-02	0	0	1.91e+03	1.22e+03	1.88e+02	0	0	0
ZH ($H\tau\tau$)	6.10e+02	2.03e+02	6.46e+01	1.65e+03	1.11e+03	1.77e+02	2.07e+03	1.35e+03	2.52e+02
$H \to$ non-$\tau\tau$	6.34e+01	6.55e+01	1.66e+02	7.19e+01	3.05e+02	4.56e+02	2.41e+03	1.78e+03	8.51e+03
DY	1.73e+02	1.60e+01	5.77e+01	1.82e+06	1.60e+06	8.42e+06	3.16e+05	3.50e+03	1.46e+04
WW	5.78e+01	9.12e+01	2.90e+02	1.29e+05	8.83e+05	1.52e+06	3.19e+05	5.54e+05	8.00e+02
ZZ	3.12e+03	1.17e+03	7.58e+03	8.86e+03	6.82e+03	4.37e+04	2.41e+04	1.51e+04	7.73e+04
$t\bar{t}$	5.99e+00	0	0	0	2.82e+00	2.82e+00	5.87e+03	3.38e+04	4.97e+04
$ee \to \nu\nu Z$	0	0	0	4.80e+03	2.74e+03	2.18e+04	2.29e+03	5.94e+00	0
$e\gamma \to eZ$	0	0	4.19e-01	6.91e+01	1.35e+04	6.44e+05	0	7.13e+00	5.93e+02
$\gamma\gamma \to \ell\ell$	0	0	0	2.45e+02	5.16e+04	2.41e+06	0	0	7.72e+00
$\gamma\gamma \to \tau\tau$	0	0	0	0	0	0	0	0	0

Table 24: Table of expected yields of signal and background processes after category selection at $\sqrt{s} = 365$ GeV with $\mathcal{L} = 3$ ab^{-1} for explicit tau reconstruction using inclusive jets.

	$\ell\ell\tau_h\tau_h$	$\ell\ell\tau_\ell\tau_h$	$\ell\ell\tau_\ell\tau_\ell$	$\nu\nu\tau_h\tau_h$	$\nu\nu\tau_\ell\tau_h$	$\nu\nu\tau_\ell\tau_\ell$	$qq\tau_h\tau_h$	$qq\tau_\ell\tau_h$	$qq\tau_\ell\tau_\ell$
VBF $H \to \tau\tau$	1.50e-02	0	0	1.80e+03	9.34e+02	1.88e+02	3.38e+02	3.25e+01	7.03e-03
ZH ($H\tau\tau$)	5.57e+02	1.60e+02	6.46e+01	1.67e+03	1.08e+03	1.77e+02	4.51e+03	2.92e+03	5.17e+02
$H \to$ non-$\tau\tau$	8.96e+01	9.66e+01	1.66e+02	2.71e+02	9.15e+02	4.56e+02	8.60e+03	5.65e+03	2.34e+04
DY	1.75e+02	1.58e+01	5.77e+01	1.66e+06	1.21e+06	8.42e+06	3.89e+06	4.33e+04	2.52e+04
WW	7.16e+01	6.46e+01	2.90e+02	1.86e+05	1.00e+06	1.52e+06	9.84e+05	1.84e+06	3.81e+03
ZZ	3.22e+03	8.22e+02	7.58e+03	1.10e+04	8.14e+03	4.37e+04	8.60e+04	2.63e+04	1.33e+05
$t\bar{t}$	7.99e+00	0	0	2.40e+02	4.42e+03	2.82e+00	2.07e+04	1.03e+05	8.89e+04
$ee \to \nu\nu Z$	0	0	0	5.17e+03	1.75e+03	2.18e+04	2.85e+04	7.72e+01	3.78e-01
$e\gamma \to eZ$	0	0	4.19e-01	1.77e+01	3.58e+03	6.44e+05	0	2.11e+01	2.45e+03
$\gamma\gamma \to \ell\ell$	0	0	0	3.78e+01	7.10e+03	2.41e+06	0	0	1.10e+01
$\gamma\gamma \to \tau\tau$	0	0	0	0	0	0	0	0	0

Table 25: Table of expected yields of signal and background processes after category selection at $\sqrt{s} = 365$ GeV with $\mathcal{L} = 3$ ab^{-1} for explicit tau reconstruction using exclusive jets.

	$\ell\ell\tau_h\tau_h$	$\ell\ell\tau_\ell\tau_h$	$\ell\ell\tau_\ell\tau_\ell$	$\nu\nu\tau_h\tau_h$	$\nu\nu\tau_\ell\tau_h$	$\nu\nu\tau_\ell\tau_\ell$	$qq\tau_h\tau_h$	$qq\tau_\ell\tau_h$	$qq\tau_\ell\tau_\ell$
VBF $H \to \tau\tau$	1.31e-02	0	0	3.34e+03	1.58e+03	1.88e+02	0	0	0
ZH ($H\tau\tau$)	1.06e+03	2.65e+02	6.46e+01	2.78e+03	1.43e+03	1.77e+02	3.48e+03	1.85e+03	2.19e+02
$H \to$ non-$\tau\tau$	1.79e+02	1.56e+02	1.66e+02	2.73e+02	7.51e+02	4.56e+02	3.21e+03	3.53e+03	8.91e+03
DY	2.35e+02	2.12e+01	5.77e+01	2.89e+06	2.90e+06	8.42e+06	3.15e+05	1.54e+04	1.63e+04
WW	1.30e+02	1.63e+02	2.90e+02	2.44e+05	1.21e+06	1.52e+06	2.74e+05	6.95e+05	6.77e+02
ZZ	6.07e+03	3.41e+03	7.58e+03	1.69e+04	2.04e+04	4.37e+04	3.66e+04	3.92e+04	8.69e+04
$t\bar{t}$	0	0	0	4.79e+00	4.23e+00	2.82e+00	1.21e+04	4.98e+04	5.09e+04
$ee \to \nu\nu Z$	0	0	0	8.23e+03	5.88e+03	2.18e+04	1.44e+03	1.35e+01	0
$e\gamma \to eZ$	5.74e+02	4.07e+02	4.19e-01	2.07e+04	7.79e+04	6.44e+05	0	0	0
$\gamma\gamma \to \ell\ell$	7.72e+00	0	0	2.07e+04	4.11e+05	2.41e+06	0	0	0
$\gamma\gamma \to \tau\tau$	0	0	0	0	0	0	0	0	0

Table 26: Table of expected yields of signal and background processes after category selection at $\sqrt{s} = 365$ GeV with $\mathcal{L} = 3$ ab^{-1} for ParticleNet tau reconstruction using inclusive jets.

	$\ell\ell\tau_h\tau_h$	$\ell\ell\tau_\ell\tau_h$	$\ell\ell\tau_\ell\tau_\ell$	$\nu\nu\tau_h\tau_h$	$\nu\nu\tau_\ell\tau_h$	$\nu\nu\tau_\ell\tau_\ell$	$qq\tau_h\tau_h$	$qq\tau_\ell\tau_h$	$qq\tau_\ell\tau_\ell$
VBF $H \to \tau\tau$	1.31e-02	0	0	3.18e+03	1.11e+03	1.88e+02	3.05e-01	3.31e-02	0
ZH ($H\tau\tau$)	1.02e+03	2.10e+02	6.46e+01	2.65e+03	1.30e+03	1.77e+02	5.75e+03	3.48e+03	5.23e+02
$H \to$ non-$\tau\tau$	1.85e+02	1.02e+02	1.66e+02	6.94e+02	8.60e+02	4.56e+02	6.74e+03	7.21e+03	2.54e+04
DY	1.38e+03	2.06e+01	5.77e+01	2.78e+06	2.35e+06	8.42e+06	2.41e+06	2.44e+04	2.77e+04
WW	3.52e+02	1.12e+02	2.90e+02	2.63e+05	9.90e+05	1.52e+06	4.86e+05	1.17e+06	3.39e+03
ZZ	7.02e+03	2.26e+03	7.58e+03	2.28e+04	1.70e+04	4.37e+04	8.09e+04	5.89e+04	1.52e+05
$t\bar{t}$	0	0	0	5.64e+00	5.32e+00	2.82e+00	2.04e+04	7.70e+04	9.26e+04
$ee \to \nu\nu Z$	3.78e-01	0	0	7.77e+03	4.00e+03	2.18e+04	1.24e+04	2.38e+01	0
$e\gamma \to eZ$	2.38e+03	1.91e+03	4.19e-01	7.96e+03	6.93e+04	6.44e+05	0	4.19e-01	0
$\gamma\gamma \to \ell\ell$	1.10e+01	0	0	2.14e+04	2.16e+05	2.41e+06	0	0	0
$\gamma\gamma \to \tau\tau$	0	0	0	0	0	0	0	0	0

Table 27: Table of expected yields of signal and background processes after category selection at $\sqrt{s} = 365$ GeV with $\mathcal{L} = 3$ ab^{-1} for ParticleNet tau reconstruction using exclusive jets.

References

[1] G. Aad et al. "Observation of a new particle in the search for the Standard Model Higgs boson with the ATLAS detector at the LHC". In: *Phys. Lett. B* 716 (2012), pp. 1–29. DOI: 10.1016/j.physletb.2012.08.020. arXiv: 1207.7214 [hep-ex].

[2] S. Chatrchyan et al. "Observation of a New Boson at a Mass of 125 GeV with the CMS Experiment at the LHC". In: *Phys. Lett. B* 716 (2012), pp. 30–61. DOI: 10.1016/j.physletb.2012.08.021. arXiv: 1207.7235 [hep-ex].

[3] A. Abada et al. "FCC-ee: The Lepton Collider: Future Circular Collider Conceptual Design Report Volume 2". In: *Eur. Phys. J. ST* 228.2 (2019), pp. 261–623. DOI: 10.1140/epjst/e2019-900045-4.

[4] A. Abada et al. "FCC Physics Opportunities: Future Circular Collider Conceptual Design Report Volume 1". In: *Eur. Phys. J. C* 79.6 (2019), p. 474. DOI: 10.1140/epjc/s10052-019-6904-3.

[5] The IDEA Study Group. *The IDEA detector concept for FCC-ee*. 2025. arXiv: 2502.21223 [physics.ins-det]. URL: https://arxiv.org/abs/2502.21223.

[6] P. Konar and A. K. Swain. "Reconstructing semi-invisible events in resonant tau pair production from Higgs". In: *Physics Letters B* 757 (2016), pp. 211–215. ISSN: 0370-2693. DOI: 10.1016/j.physletb.2016.03.070. URL: https://www.sciencedirect.com/science/article/pii/S0370269316300417.

[7] *FCC-config*. URL: https://github.com/HEP-FCC/FCC-config.

[8] *Delphes FCC-ee Physic events winter 2023 production (IDEA)*. URL: https://fcc-physics-events.web.cern.ch/FCCee/delphes/winter2023/idea/.

[9] T. Madlener et al. *key4hep/EDM4Hep*. DOI: 10.5281/zenodo.4785062.

[10] W. Kilian, T. Ohl, and J. Reuter. "WHIZARD: Simulating Multi-Particle Processes at LHC and ILC". In: *Eur. Phys. J. C* 71 (2011), p. 1742. DOI: 10.1140/epjc/s10052-011-1742-y. arXiv: 0708.4233 [hep-ph].

[11] M. Moretti, T. Ohl, and J. Reuter. "O'Mega: An Optimizing matrix element generator". In: (Feb. 2001). Ed. by T. Behnke et al., pp. 1981–2009. arXiv: hep-ph/0102195.

[12] T. Sjostrand, S. Mrenna, and P. Z. Skands. "PYTHIA 6.4 Physics and Manual". In: *JHEP* 05 (2006), p. 026. DOI: 10.1088/1126-6708/2006/05/026. arXiv: hep-ph/0603175.

[13] J. de Favereau et al. "DELPHES 3, A modular framework for fast simulation of a generic collider experiment". In: *JHEP* 02 (2014), p. 057. DOI: 10.1007/JHEP02(2014)057. arXiv: 1307.6346 [hep-ex].

[14] *FCCAnalyses*. URL: https://github.com/HEP-FCC/FCCAnalyses.

[15] M. Cacciari, G. P. Salam, and G. Soyez. "FastJet User Manual". In: *Eur. Phys. J. C* 72 (2012), p. 1896. DOI: 10.1140/epjc/s10052-012-1896-2. arXiv: 1111.6097 [hep-ph].

[16] Franco Bedeschi, Loukas Gouskos, and Michele Selvaggi. "Jet flavour tagging for future colliders with fast simulation". In: *The European Physical Journal C* 82.7 (July 2022). ISSN: 1434-6052. DOI: 10.1140/epjc/s10052-022-10609-1. URL: http://dx.doi.org/10.1140/epjc/s10052-022-10609-1.

[17] A. Hayrapetyan et al. "The CMS Statistical Analysis and Combination Tool: COMBINE". In: *Submitted to Computing and Software for Big Science* (Apr. 2024). arXiv: 2404.06614 [physics.data-an].

[18] R. J. Barlow and C. Beeston. "Fitting using finite Monte Carlo samples". In: *Comput. Phys. Commun.* 77 (1993), pp. 219–228. DOI: 10.1016/0010-4655(93)90005-W.